Composite Materials and Engineering, *Vol. 2, No. 1 (2020) 25-41*
DOI: https://doi.org/10.12989/cme.2020.2.1.025

Modeling and evaluation of rectangular hole effect on nonlinear behavior of imperfect composite plates by an effective simulation technique

S.A.M. Ghannadpour* and M. Mehrparvar

New Technologies and Engineering Department, Shahid Beheshti University, G.C, Tehran, Iran

(Received August 12, 2019, Revised October 7, 2019, Accepted October 8, 2019)

Abstract. In the present study, geometrically nonlinear behavior of relatively thick composite laminates containing square and rectangular cutouts with or without initial geometric imperfection has been investigated. The effects of cutout size, shape and presence of initial geometric imperfection for plates under uniaxial in-plane compressive load are studied. The structural model is based on the first-order shear deformation theory and Von-Karman's assumptions are used to incorporate geometric nonlinearity. The perforated plate is modeled by assembling eight plate-elements and the connection between these elements is provided by the Penalty method, which is called plate assembly technique. The fundamental equations for perforated plates are obtained by the principle of minimum of total potential energy and the response is found by solving the obtained nonlinear set of equations using the quadratic extrapolation technique. The approximation of the displacement fields in this study has been based on the Ritz method and by Chebyshev polynomials. The load-displacement responses for plates with various cutouts and with different boundary conditions are extensively provided. The accuracy of the present work is examined by comparing the results with the finite element analyses by ABAQUS program wherever possible.

Keywords: geometrically nonlinear behavior; square/rectangular cutouts; composite laminates; plate assembly technique; penalty method

1. Introduction

Composite structures are subject of many studies and used as structural components in many industries especially aerospace industries due to their light weight and durability. By piling layers with different material properties and various fiber orientation, the composite laminates are fabricated. Composite laminate's planer dimensions are one or two orders of magnitude larger than the laminate thickness. For moderately thick plates, the transversal shear effect should be taken into account, as a result, the first-order shear deformation theory (FSDT) is used in this paper. Reddy (2004) described the laminated plates mechanics and theories in details in his book. These composite components are often in situations where they are subjected to in-plane compressive loading. Consequently, it is a necessity to precisely foresee the buckling of such elements and many studies have been done in this field for instance, Ghannadpour and Ovesy (2009) used the exact finite strip

*Corresponding author, Ph.D., E-mail: a_ghannadpour@sbu.ac.ir

http://www.techno-press.org/?journal=cme&subpage=7 ISSN: 2671-4930 (Print), 2671-5120 (Online)

method to investigate the buckling of composite plate using classical laminate theory (CLPT). The free vibration and buckling responses of laminated plates based on first-order shear deformation mesh-free method has been done by Liew *et al*. (2004). An inclusive review in the field of buckling has been done by Leissa (1987). Yang *et al*. (2013) investigated the buckling and ultimate strength of laminates under compression. Also, many works have been done for plates in thermal environments for example, Kar *et al*. (2016), Katariya *et al*. (2017), Kandasamy *et al*. (2016), Katariya and Panda (2016), Tounsi *et al*. (2019).

Alternatively, plates may tolerate additional loads even after buckling happens and hence predicting the buckling and post-buckling response of such structures precisely is a research interest. Chia (1988) has done a comprehensive review in the field of post-buckling and Ghannadpour *et al*. (2015, 2016, 2011) established a new exact finite strip based on FSDT to analyze the buckling and post-buckling behavior of laminates and channel section struts.

Similarly, many studies have been done on structures under other sort of loading for instance, Brubak and Hellesland (2007) used a semi-analytical approach to study nonlinear behavior of stiffened plates under bending and for plates under thermal loading, Panda and Singh (2009, 2010 and 2013) have done many investigations. Many methods have been employed to study the nonlinear response of composite plates like, Yang and Hayman (2015), Noor and Peters (1994), Cetkovic and Vuksanovic (2011), Ghannadpour and Kiani (2018), Ghannadpour *et al*. (2018).

Also, perforated plates are vastly deployed as structural members to further reduce the weight of structures, openings for hardware and wiring to pass through and in case of fuselage windows and doors. Investigating the buckling of structures is a necessity since the occurrence of the cutouts may cause the plates stability reduces significantly and reallocate the membrane stresses in the plates, therefore the stability of mentioned structures should be calculated. Britt (1994) studied panels with elliptical cutouts located at center under compression and shear loadings and the principle of minimum potential energy is used to acquire the buckling solution. Moreover, many other works has been done throughout the past years to study the buckling behavior of plates, one can point out the work Eiblmeier and Loughlan (1995) in which NASTRAN finite element analysis has been used, and thermal buckling response has been studied by Şahin (2005).

Ghannadpour *et al*. (2006) used finite element method to study the buckling behavior of cross-ply laminated plates with circular and elliptical cutouts and there are many other works in this field, such as Baba and Baltaci (2007), Komur and Sonmez (2008), Komur *et al*. (2010).

And in case of post-buckling phase, as previously mentioned, the structures may enter this phase since they could endure higher load than the buckling load thus, doing studies in this field is inevitable to completely utilize the stability of the plate. So, nonlinear post-buckling behavior of the plates with cutouts is a research interest, Mohammadi *et al*. (2006) explored the pre- and post-buckling and effective width of laminates with compressive loading. The post-buckling response of isotropic and laminated plates with circular holes has been carried out by Vandenbrink and Kamat (1987) and Nemeth (1990) done an experimental study of buckling and post-buckling behavior of perforated composite plates with different layups. In addition to the above investigations, many other works have been carried out to study the nonlinear or post-buckling behavior of perforated plates such as Madenci and Barut (1994), Kong *et al*. (2001), Jain and Kumar (2004), Bakhshi and Taheri-Behrooz (2019).

Recently, Ghannadpour and Mehrparvar (2018a) introduced energy effect removal technique to investigate the post-buckling behavior of composite plates which contain circular/ elliptical cutouts. In another study, they used the so called plate assembly technique to analyze the nonlinear behavior of functionally graded plates containing rectangular cutouts in which case the Penalty method was

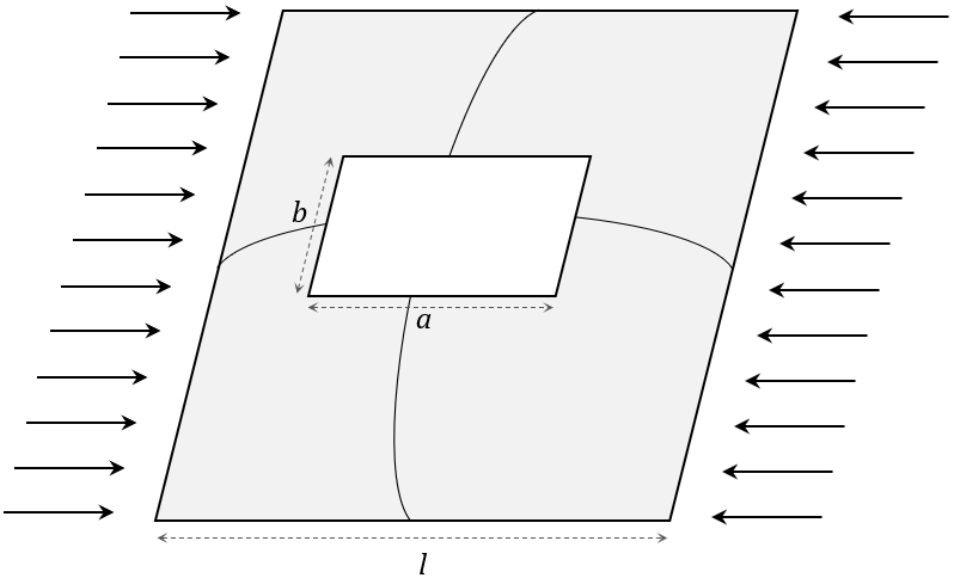

Fig. 1 A typical perforated square plate with initial imperfection

employed to model perforated plate (Ghannadpour and Mehrparvar 2018b).

In the current study, the geometrically nonlinear analysis of perforated laminates with or without initial geometric imperfection has been carried out under the in-plane compressive load. The solution is based on FSDT and Von-Karman's assumptions. Penalty method is used to assemble the perforated plate by connecting eight plate-elements. The approximation of the displacement fields in this study has been based on the Ritz technique and by Chebyshev polynomials. The fundamental equations of laminates containing cutout are obtained by the principle of minimum of total potential energy and the response is found by solving the obtained nonlinear set of equations using the quadratic extrapolation technique. The effects of cutout size, shape and presence of initial geometric imperfection for plates under uniaxial in-plane compressive load are being investigated. The accuracy of the present work is examined by comparing the results with the finite element analyses by ABAQUS program wherever possible.

2. Formulation development

A typical perforated square laminate of dimensions $l \times l$, total thickness h and cutout of dimensions $a \times b$ is shown in Fig. 1. The plate is subjected to in-plane compressive loads normal to the edges $x = \pm l/2$. The boundary conditions are chosen to be simply supported on all edges.

The perforated composite plate shown in Fig. 1 is assembled by eight plate-elements and this can be shown in the formulation by the superscript (i) associated with the $(i)^{th}$ element, as shown in Fig. 2.

In the current study, the laminated plates deform under compressive loads and then each point in the domain of the plates with the position vector $\boldsymbol{x}$ is transferred to a new coordinate value $\boldsymbol{x}^*$

$$\boldsymbol{x} = \langle x \quad y \quad z \rangle^T \implies \boldsymbol{x}^* = \langle x^* \quad y^* \quad z^* \rangle^T \qquad \text{by} \qquad \boldsymbol{x}^* = \boldsymbol{x} + \boldsymbol{u} \tag{1}$$

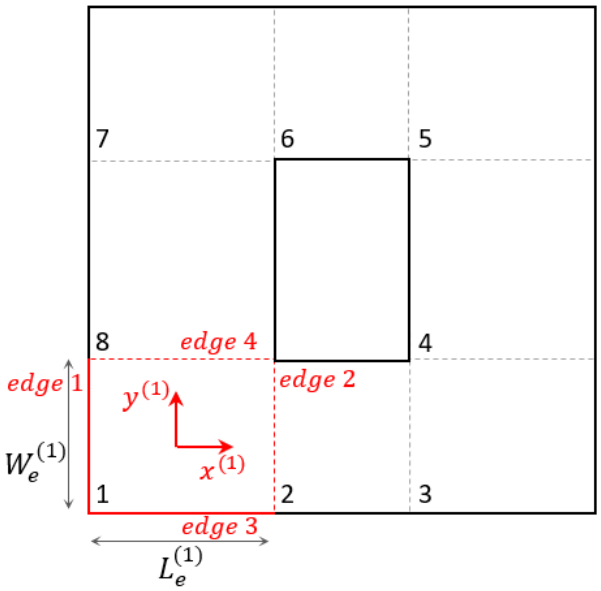

Fig. 2 Assembly of the plate-elements to model the perforated laminate

Where the displacement vector $\boldsymbol{u} = \langle \bar{u} \quad \bar{v} \quad \bar{w} \rangle^T$ defines the deformation of a laminated plate whose components are given by

$$\begin{aligned} \bar{u}(x,y,z) &= u(x,y) + z\varphi_x(x,y) \\ \bar{v}(x,y,z) &= v(x,y) + z\varphi_y(x,y) \\ \bar{w}(x,y,z) &= w(x,y) + w_I(x,y) \end{aligned} \tag{2}$$

According to the first-order shear deformation theory, u, v and w are in-plane and out-of-plane displacements of mid-plane, and φ_x and φ_y symbolize the rotations of a transverse normal about axes parallel to the x and y axes, respectively. Also, the effect of initial geometric imperfection, as shown by w_I, is applied in the z-direction and therefore the effect of this imperfection is also included in the third equation of relations (2).

As mentioned before and according to Fig. 2, in order to investigate the behavior of laminated plate, that is divided into 8 plate-elements, all above displacement fields $u, v,\ w, \varphi_x$ and φ_y which should be approximated in the domain of the plate are in fact approximated separately for each plate-element. These displacement functions should satisfy the essential boundary conditions of the problem which in this study the boundary conditions of laminates are chosen to be simply supported on all edges. Also, the longitudinal displacement along the x-direction at $x = \pm l/2$ are allowed and assumed to be straight and for lateral expansion at $y = \pm l/2$, the plate is considered to move freely. Thus, the displacement fields for each plate-element can be written as

$$\tau^{(i)}(x,y) = \mathbb{B}_\tau^{(i)}(x,y) \sum_{m=1}^{N_t} \sum_{n=1}^{N_t} \delta_{mn}^{\tau^{(i)}} T_{m-1}\left(\frac{2x}{L_e^{(i)}}\right) T_{n-1}\left(\frac{2y}{W_e^{(i)}}\right) + f_\tau^{(i)}(x,y)\delta_c^{\tau^{(i)}}, \quad i = 1,2,\ldots,8 \tag{3}$$

Where $\tau \in \{u, v, w, \varphi_x, \varphi_y\}$ is a selected displacement field for $(i)^{th}$ plate-element and N_t is the number of terms in series expansion which in the current work has the same value for all

displacement fields and plate-elements. The coefficients δ_{mn}^{τ} and δ_{c}^{τ} are the Ritz unknown coefficients of the problem for each plate-element (i) and the latter is for satisfying the straight conditions mentioned previously. It is noted that the origin of the coordinates for each plate-element is assumed to be at its center as in Fig. 2.

The term $\mathbb{B}_{\tau}(x,y)$ in Eq. (3) is the boundary function and is chosen to guarantee the contentment of the essential boundary conditions of each plate-element (i). It can be defined as

$$\mathbb{B}_{\tau}^{(i)}(x,y)=\prod_{\beta=1,2}\left(1+(-1)^{\beta-1}\left(\frac{2x}{L_e^{(i)}}\right)\right)^{\mu_{\beta}^{\tau(i)}}\prod_{\beta=3,4}\left(1+(-1)^{\beta-1}\left(\frac{2y}{W_e^{(i)}}\right)\right)^{\mu_{\beta}^{\tau(i)}},\ i=1,\dots,8 \tag{4}$$

Where β denotes the edge number, shown in Fig. 2, and the exponents $\mu_{\beta}^{\tau(i)}$ can take value 0 for free condition and value 1 according to the conditions of held (or straight) for each displacement field $\tau\in\{u,v,w,\varphi_x,\varphi_y\}$ and for each plate-element.

The boundary function $f_{\tau}^{(i)}(x,y)$ is also chosen to guarantee the contentment of the straight boundary conditions of the plates as mentioned before. Therefore, since this specified boundary condition is only related to the in-plane displacement field u, the value of this function is zero for other displacement fields, $\tau\in\{v,w,\varphi_x,\varphi_y\}$.

As it is seen in Eq. (3), the approximation of displacement fields is performed by Chebyshev polynomials. Chebyshev differential equation is written as

$$(1-x^2)\frac{d^2y}{dx^2}-x\frac{dy}{dx}+n^2y=0 \qquad n=0,1,2,3,\dots \tag{5}$$

The n^{th}Chebyshev polynomial of the first kind, denoted by $T_n(x)$ is defined as

$$T_n(x)=\cos(n\cos^{-1}x) \tag{6}$$

By establishment of the displacement functions approximation as defined above, the in-plane strain vectors for each plate-element can be represented as

$$\bar{\boldsymbol{\varepsilon}}^{(i)}=\begin{Bmatrix}\bar{\varepsilon}_{xx}^{(i)}\\ \bar{\varepsilon}_{yy}^{(i)}\\ \bar{\varepsilon}_{xy}^{(i)}\end{Bmatrix}=\boldsymbol{\varepsilon}^{(i)}+z\boldsymbol{\psi}^{(i)},\quad \boldsymbol{\varepsilon}^{(i)}=\begin{Bmatrix}\varepsilon_{xx}^{(i)}\\ \varepsilon_{yy}^{(i)}\\ \varepsilon_{xy}^{(i)}\end{Bmatrix}=\boldsymbol{\varepsilon}_{\boldsymbol{l}}^{(i)}+\boldsymbol{\varepsilon}_{\boldsymbol{nl}}^{(i)}+\boldsymbol{\varepsilon}_{\boldsymbol{I}}^{(i)} \tag{7}$$

where $\boldsymbol{\varepsilon}_{\boldsymbol{l}}^{(i)}$, $\boldsymbol{\varepsilon}_{\boldsymbol{nl}}^{(i)}$and $\boldsymbol{\varepsilon}_{\boldsymbol{I}}^{(i)}$are linear and nonlinear strain vectors and strain vector for initial geometric imperfection for $(i)^{th}$ plate-element, respectively. Also, the vectors $\boldsymbol{\psi}^{(i)}$ and $\boldsymbol{\varepsilon}_{\boldsymbol{s}}^{(i)}$are respectively curvature and shear strains vectors, and they can be defined as

$$\boldsymbol{\varepsilon}_{\boldsymbol{l}}^{(i)}=\begin{Bmatrix}\dfrac{\partial u^{(i)}}{\partial x}\\ \dfrac{\partial v^{(i)}}{\partial y}\\ \dfrac{\partial u^{(i)}}{\partial y}+\dfrac{\partial v^{(i)}}{\partial x}\end{Bmatrix},\quad \boldsymbol{\varepsilon}_{\boldsymbol{nl}}^{(i)}=\begin{Bmatrix}\dfrac{1}{2}\left(\dfrac{\partial w^{(i)}}{\partial x}\right)^2\\ \dfrac{1}{2}\left(\dfrac{\partial w^{(i)}}{\partial y}\right)^2\\ \dfrac{\partial w^{(i)}}{\partial x}\dfrac{\partial w^{(i)}}{\partial y}\end{Bmatrix},$$

$$\boldsymbol{\varepsilon}_{\boldsymbol{I}}^{(i)} = \begin{Bmatrix} \dfrac{\partial w^{(i)}}{\partial x}\dfrac{\partial w_I^{(i)}}{\partial x} \\ \dfrac{\partial w^{(i)}}{\partial y}\dfrac{\partial w_I^{(i)}}{\partial y} \\ \dfrac{\partial w^{(i)}}{\partial x}\dfrac{\partial w_I^{(i)}}{\partial y} + \dfrac{\partial w^{(i)}}{\partial y}\dfrac{\partial w_I^{(i)}}{\partial x} \end{Bmatrix} \tag{8}$$

and

$$\boldsymbol{\psi}^{(i)} = \begin{Bmatrix} \dfrac{\partial \varphi_x^{(i)}}{\partial x} \\ \dfrac{\partial \varphi_y^{(i)}}{\partial y} \\ \dfrac{\partial \varphi_x^{(i)}}{\partial y} + \dfrac{\partial \varphi_y^{(i)}}{\partial x} \end{Bmatrix}, \boldsymbol{\varepsilon}_{\boldsymbol{s}}^{(i)} = \begin{Bmatrix} \varphi_y^{(i)} + \dfrac{\partial w^{(i)}}{\partial y} \\ \varphi_x^{(i)} + \dfrac{\partial w^{(i)}}{\partial x} \end{Bmatrix} \tag{9}$$

With the assumption that each layer is in a condition of plane stress, stress-strain relationships for each lamina at a general point and for each plate-element are written as below

$$\boldsymbol{\sigma}^{(i)} = \begin{Bmatrix} \sigma_{xx}^{(i)} \\ \sigma_{yy}^{(i)} \\ \tau_{xy}^{(i)} \end{Bmatrix} = \begin{bmatrix} \bar{Q}_{11} & \bar{Q}_{12} & \bar{Q}_{16} \\ \bar{Q}_{12} & \bar{Q}_{22} & \bar{Q}_{26} \\ \bar{Q}_{16} & \bar{Q}_{26} & \bar{Q}_{66} \end{bmatrix}^{(i)} \begin{Bmatrix} \bar{\varepsilon}_{xx}^{(i)} \\ \bar{\varepsilon}_{yy}^{(i)} \\ \bar{\varepsilon}_{xy}^{(i)} \end{Bmatrix} = \overline{\boldsymbol{Q}}^{(i)} \bar{\boldsymbol{\varepsilon}}^{(i)} \tag{10}$$

$$\boldsymbol{\sigma}_{\boldsymbol{s}}^{(i)} = \begin{bmatrix} \bar{Q}_{44} & \bar{Q}_{45} \\ \bar{Q}_{45} & \bar{Q}_{55} \end{bmatrix}^{(i)} \begin{Bmatrix} \varphi_y^{(i)} + \dfrac{\partial w^{(i)}}{\partial y} \\ \varphi_x^{(i)} + \dfrac{\partial w^{(i)}}{\partial x} \end{Bmatrix} = \overline{\boldsymbol{Q}}_{\boldsymbol{s}}^{(i)} \boldsymbol{\varepsilon}_{\boldsymbol{s}}^{(i)} \tag{11}$$

Where $\overline{\boldsymbol{Q}}^{(i)}$ is transformed reduced stiffness matrix and $\overline{\boldsymbol{Q}}_{\boldsymbol{s}}^{(i)}$ is transformed shear stiffness matrix for $(i)^{th}$ plate-element. Each composite plate-element has its stiffness matrices $\boldsymbol{A}^{(i)}, \boldsymbol{B}^{(i)}, \boldsymbol{D}^{(i)}, \boldsymbol{A}_{\boldsymbol{s}}^{(i)}$ that their coefficients can be obtained by

$$\left(\boldsymbol{A}_{pq}^{(i)}, \boldsymbol{B}_{pq}^{(i)}, \boldsymbol{D}_{pq}^{(i)}\right) = \int_{-h/2}^{h/2} \overline{\boldsymbol{Q}}_{pq}^{(i)} (1, z, z^2) dz, \;\; p, q = 1,2,3 \tag{12}$$

$$\boldsymbol{A}_{\boldsymbol{s}_{pq}}^{(i)} = k_s \int_{-h/2}^{h/2} \overline{\boldsymbol{Q}}_{\boldsymbol{s}_{pq}}^{(i)} dz, \;\; p, q = 1,2 \tag{13}$$

where k_s is the shear correction factor and it's chosen to be 5/6 in this study. With the above explanations, the total potential energy of $(i)^{th}$ plate-element can be obtained. First of all, the strain energy related to the in-plane stresses for $(i)^{th}$ plate-element with volume $V^{(i)}$and surface area $\Omega^{(i)}$and by using the Eqs. (7) and (10) can be written as

$$U^{(i)} = \frac{1}{2} \iiint_{V^{(i)}} \bar{\boldsymbol{\varepsilon}}^{(i)^T} \boldsymbol{\sigma}^{(i)} \mathrm{d}V^{(i)} = \frac{1}{2} \iint_{\Omega^{(i)}} \int_{-h/2}^{+h/2} \bar{\boldsymbol{\varepsilon}}^{(i)^T} \overline{\boldsymbol{Q}}^{(i)} \bar{\boldsymbol{\varepsilon}}^{(i)} \mathrm{d}z \, \mathrm{d}\Omega^{(i)}$$

$$= \frac{1}{2}\iint_{\Omega^{(i)}}\int_{-h/2}^{+h/2}\left(\boldsymbol{\varepsilon}_{\boldsymbol{l}}^{(i)}+\boldsymbol{\varepsilon}_{\boldsymbol{nl}}^{(i)}+\boldsymbol{\varepsilon}_{\boldsymbol{I}}^{(i)}+z\boldsymbol{\psi}^{(i)}\right)^{T}\overline{\boldsymbol{Q}}^{(i)}\left(\boldsymbol{\varepsilon}_{\boldsymbol{l}}^{(i)}+\boldsymbol{\varepsilon}_{\boldsymbol{nl}}^{(i)}+\boldsymbol{\varepsilon}_{\boldsymbol{I}}^{(i)}+z\boldsymbol{\psi}^{(i)}\right)\mathrm{d}z\,\mathrm{d}\Omega^{(i)} \tag{14}$$

By integrating through the thickness with respect to *z* from the Eq. (14) and substituting Eq. (12) into Eq. (14), the strain energy can be rewritten as

$$\begin{aligned}U^{(i)} = \iint_{\Omega^{(i)}}\Big(&\frac{1}{2}\boldsymbol{\varepsilon}_{\boldsymbol{l}}^{(i)^T}\boldsymbol{A}^{(i)}\boldsymbol{\varepsilon}_{\boldsymbol{l}}^{(i)}+\boldsymbol{\varepsilon}_{\boldsymbol{l}}^{(i)^T}\boldsymbol{A}^{(i)}\boldsymbol{\varepsilon}_{\boldsymbol{nl}}^{(i)}+\frac{1}{2}\boldsymbol{\varepsilon}_{\boldsymbol{nl}}^{(i)^T}\boldsymbol{A}^{(i)}\boldsymbol{\varepsilon}_{\boldsymbol{nl}}^{(i)}+\boldsymbol{\varepsilon}_{\boldsymbol{l}}^{(i)^T}\boldsymbol{A}^{(i)}\boldsymbol{\varepsilon}_{\boldsymbol{I}}^{(i)}\\&+\boldsymbol{\varepsilon}_{\boldsymbol{nl}}^{(i)^T}\boldsymbol{A}^{(i)}\boldsymbol{\varepsilon}_{\boldsymbol{I}}^{(i)}+\frac{1}{2}\boldsymbol{\varepsilon}_{\boldsymbol{I}}^{(i)^T}\boldsymbol{A}^{(i)}\boldsymbol{\varepsilon}_{\boldsymbol{I}}^{(i)}+\boldsymbol{\psi}^{(i)^T}\boldsymbol{B}^{(i)}\boldsymbol{\varepsilon}_{\boldsymbol{I}}^{(i)}+\boldsymbol{\varepsilon}_{\boldsymbol{l}}^{(i)^T}\boldsymbol{B}^{(i)}\boldsymbol{\psi}^{(i)}\\&+\boldsymbol{\varepsilon}_{\boldsymbol{nl}}^{(i)^T}\boldsymbol{B}^{(i)}\boldsymbol{\psi}^{(i)}+\frac{1}{2}\boldsymbol{\psi}^{(i)^T}\boldsymbol{D}^{(i)}\boldsymbol{\psi}^{(i)}\Big)\mathrm{d}\Omega^{(i)}, i=1,\dots,8\end{aligned} \tag{15}$$

Then, shear strain energy $U_s$for $(i)^{th}$ plate-element should be computed. It can be obtained by the following relation and by using the Eqs. (9), (11) and (13).

$$\begin{aligned}U_s^{(i)} &= \frac{1}{2}\iiint_{V^{(i)}}\boldsymbol{\varepsilon}_{\boldsymbol{s}}^{(i)^T}\boldsymbol{\sigma}_{\boldsymbol{s}}^{(i)}\mathrm{d}V^{(i)} = \frac{1}{2}\iint_{\Omega^{(i)}}\int_{-h/2}^{+h/2}\boldsymbol{\varepsilon}_{\boldsymbol{s}}^{(i)^T}\overline{\boldsymbol{Q}}_{\boldsymbol{s}}^{(i)}\boldsymbol{\varepsilon}_{\boldsymbol{s}}^{(i)}\mathrm{d}z\,\mathrm{d}\Omega^{(i)}\\&= \frac{1}{2}\iint_{\Omega^{(i)}}\left(\boldsymbol{\varepsilon}_{\boldsymbol{s}}^{(i)^T}\boldsymbol{A}_{\boldsymbol{s}}^{(i)}\boldsymbol{\varepsilon}_{\boldsymbol{s}}^{(i)}\right)\mathrm{d}\Omega^{(i)}, i=1,\dots,8\end{aligned} \tag{16}$$

With regard to the above relations, the total strain energy of the plate can be computed by the summation of the strain energies of plate-elements. In calculating the total potential energy of each plate-element, in addition to the strain energy, it is also necessary to calculate the potential energy of external forces $V_F^{(i)}$. As presented in Fig. 1, the in-plane compressive load, N_x, is applied to the laminate and it can be calculated as

$$V_F^{(i)} = \begin{cases}\dfrac{W_e^{(i)}}{l}N_x u^{(i)}\Big|_{x=-L_e^{(i)}/2} & i=1,7,8\\ -\dfrac{W_e^{(i)}}{l}N_x u^{(i)}\Big|_{x=L_e^{(i)}/2} & i=3,4,5\end{cases} \tag{17}$$

In conclusion, the total potential energy for each plate-element is equal to the summation of the strain energies of those plate-elements with the potential energy of the applied load $V_F^{(i)}$. The total potential energy of the perforated laminated plates can also be computed by the summation of the total potential energies of the plate-elements.

However, since the entire domain of the laminates in this study has been partitioned into several plate-elements using the plate assembly technique, therefore the interface continuity between the plate-elements should be enforced wherever it is needed, for instance between 1st and 2nd elements shown in Fig. 3. For the plate-element layout presented in Fig. 2 they can be shown as

$$\begin{aligned}\tau^{(1)}\left(L_e^{(1)}/2, y\right) &= \tau^{(2)}\left(-L_e^{(2)}/2, y\right)\\ \tau^{(1)}\left(x, W_e^{(1)}/2\right) &= \tau^{(8)}\left(x, -W_e^{(8)}/2\right)\\ \tau^{(2)}\left(L_e^{(2)}/2, y\right) &= \tau^{(3)}\left(-L_e^{(3)}/2, y\right)\\ \tau^{(3)}\left(x, W_e^{(3)}/2\right) &= \tau^{(4)}\left(x, -W_e^{(4)}/2\right)\end{aligned}$$

$$\begin{aligned}
\tau^{(4)}\left(x, W_e^{(4)}/2\right) &= \tau^{(5)}\left(x, -W_e^{(5)}/2\right) \\
\tau^{(5)}\left(-L_e^{(5)}/2, y\right) &= \tau^{(6)}\left(L_e^{(6)}/2, y\right) \\
\tau^{(6)}\left(-L_e^{(6)}/2, y\right) &= \tau^{(7)}\left(L_e^{(7)}/2, y\right) \\
\tau^{(7)}\left(x, -W_e^{(7)}/2\right) &= \tau^{(8)}\left(x, W_e^{(8)}/2\right)
\end{aligned} \tag{18}$$

Where $\tau \in \{u, v, w, \varphi_x, \varphi_y\}$. As mentioned before, penalty technique is used here to apply displacement continuity along the edges shared between the plate-elements (Ghannadpour and Karimi 2018). Therefore, the equilibrium equations of the perforated plate are obtained by imposing the stationary of total potential energy under the constraints presented in Eq. (18). The enforcement of these constraints is accomplished by introducing the following penalty terms into the total potential energy functional. Thus, the penalty terms associated with Eq. (18) can be obtained by

$$\begin{aligned}
P_{1,2}^{\langle\tau\rangle} &= \frac{\gamma_{1,2}^{\langle\tau\rangle}}{2}\int_{-L_e^{(1)}/2}^{L_e^{(1)}/2}\left(\tau^{(1)}\left(L_e^{(1)}/2, y\right) - \tau^{(2)}\left(-L_e^{(2)}/2, y\right)\right)^2 \mathrm{d}y \\
P_{1,8}^{\langle\tau\rangle} &= \frac{\gamma_{1,8}^{\langle\tau\rangle}}{2}\int_{-W_e^{(1)}/2}^{W_e^{(1)}/2}\left(\tau^{(1)}\left(x, W_e^{(1)}/2\right) - \tau^{(8)}\left(x, -W_e^{(8)}/2\right)\right)^2 \mathrm{d}x \\
P_{2,3}^{\langle\tau\rangle} &= \frac{\gamma_{2,3}^{\langle\tau\rangle}}{2}\int_{-L_e^{(2)}/2}^{L_e^{(2)}/2}\left(\tau^{(2)}\left(L_e^{(2)}/2, y\right) - \tau^{(3)}\left(-L_e^{(3)}/2, y\right)\right)^2 \mathrm{d}y \\
P_{3,4}^{\langle\tau\rangle} &= \frac{\gamma_{3,4}^{\langle\tau\rangle}}{2}\int_{-W_e^{(3)}/2}^{W_e^{(3)}/2}\left(\tau^{(3)}\left(x, W_e^{(3)}/2\right) - \tau^{(4)}\left(x, -W_e^{(4)}/2\right)\right)^2 \mathrm{d}x \\
P_{4,5}^{\langle\tau\rangle} &= \frac{\gamma_{4,5}^{\langle\tau\rangle}}{2}\int_{-W_e^{(4)}/2}^{W_e^{(4)}/2}\left(\tau^{(4)}\left(x, W_e^{(4)}/2\right) - \tau^{(5)}\left(x, -W_e^{(5)}/2\right)\right)^2 \mathrm{d}x \\
P_{5,6}^{\langle\tau\rangle} &= \frac{\gamma_{5,6}^{\langle\tau\rangle}}{2}\int_{-L_e^{(5)}/2}^{L_e^{(5)}/2}\left(\tau^{(5)}\left(-L_e^{(5)}/2, y\right) - \tau^{(6)}\left(L_e^{(6)}/2, y\right)\right)^2 \mathrm{d}y \\
P_{6,7}^{\langle\tau\rangle} &= \frac{\gamma_{6,7}^{\langle\tau\rangle}}{2}\int_{-L_e^{(6)}/2}^{L_e^{(6)}/2}\left(\tau^{(6)}\left(-L_e^{(6)}/2, y\right) - \tau^{(7)}\left(L_e^{(7)}/2, y\right)\right)^2 \mathrm{d}y \\
P_{7,8}^{\langle\tau\rangle} &= \frac{\gamma_{7,8}^{\langle\tau\rangle}}{2}\int_{-W_e^{(7)}/2}^{W_e^{(7)}/2}\left(\tau^{(7)}\left(x, -W_e^{(7)}/2\right) - \tau^{(8)}\left(x, W_e^{(8)}/2\right)\right)^2 \mathrm{d}x
\end{aligned} \tag{19}$$

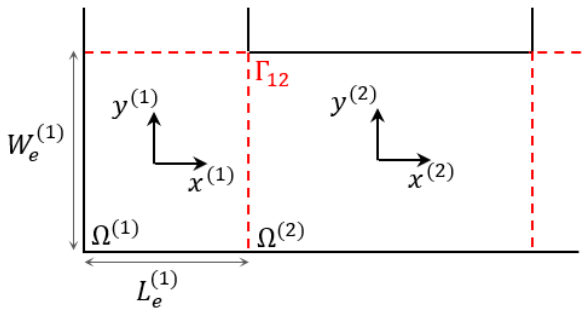

Fig. 3 Geometry configuration of shared edge between 1st and 2nd elements

Where $\tau \in \{u, v, w, \varphi_x, \varphi_y\}$ and γ are penalty coefficients (Ghannadpour *et al.* 2019). To conclude, a single relation can present the penalty terms.

$$P = \sum_{\tau} \left(P_{1,2}^{\langle\tau\rangle} + P_{1,8}^{\langle\tau\rangle} + P_{2,3}^{\langle\tau\rangle} + P_{3,4}^{\langle\tau\rangle} + P_{4,5}^{\langle\tau\rangle} + P_{5,6}^{\langle\tau\rangle} + P_{6,7}^{\langle\tau\rangle} + P_{7,8}^{\langle\tau\rangle} \right) \tag{20}$$

With the above descriptions, the total potential energy of a perforated plate is equal to the summation of the strain energies of the plate-elements (i.e., Eqs. (15) and (16)) with potential energies of the applied load for plate-elements (i.e., Eqs. (17)) and penalty terms associated with constraints presented in Eqs. (19).

$$\Pi = \sum_{i=1}^{8} \underbrace{\left(U^{(i)} + U_s^{(i)} + V_F^{(i)} \right)}_{\Pi^{(i)}} + P \tag{21}$$

By using the Eqs. (15) and (16), the final function for the total potential energy of the perforated laminate can be rewritten as follows.

$$\begin{aligned} \Pi = \sum_{i=1}^{8} V_F^{(i)} + \Bigg\{ P + \sum_{i=1}^{8} \iint_{\Omega^{(i)}} & \frac{1}{2} \boldsymbol{\varepsilon}_{\boldsymbol{l}}^{(i)^T} \boldsymbol{A}^{(i)} \boldsymbol{\varepsilon}_{\boldsymbol{l}}^{(i)} + \frac{1}{2} \boldsymbol{\psi}^{(i)^T} \boldsymbol{D}^{(i)} \boldsymbol{\psi}^{(i)} + \boldsymbol{\varepsilon}_{\boldsymbol{l}}^{(i)^T} \boldsymbol{B}^{(i)} \boldsymbol{\psi}^{(i)} \\ & + \frac{1}{2} \boldsymbol{\varepsilon}_{\boldsymbol{s}}^{(i)^T} \boldsymbol{A}_{\boldsymbol{s}}^{(i)} \boldsymbol{\varepsilon}_{\boldsymbol{s}}^{(i)} + \boldsymbol{\varepsilon}_{\boldsymbol{l}}^{(i)^T} \boldsymbol{A}^{(i)} \boldsymbol{\varepsilon}_{\boldsymbol{I}}^{(i)} + \frac{1}{2} \boldsymbol{\varepsilon}_{\boldsymbol{I}}^{(i)^T} \boldsymbol{A}^{(i)} \boldsymbol{\varepsilon}_{\boldsymbol{I}}^{(i)} + \boldsymbol{\psi}^{(i)^T} \boldsymbol{B}^{(i)} \boldsymbol{\varepsilon}_{\boldsymbol{I}}^{(i)} \Big) \mathrm{d}\Omega^{(i)} \Big) \Bigg\} \\ + \sum_{i=1}^{8} \left(\iint_{\Omega^{(i)}} \left(\boldsymbol{\varepsilon}_{\boldsymbol{l}}^{(i)^T} \boldsymbol{A}^{(i)} \boldsymbol{\varepsilon}_{\boldsymbol{nl}}^{(i)} + \boldsymbol{\varepsilon}_{\boldsymbol{nl}}^{(i)^T} \boldsymbol{B}^{(i)} \boldsymbol{\psi}^{(i)} + \boldsymbol{\varepsilon}_{\boldsymbol{nl}}^{(i)^T} \boldsymbol{A}^{(i)} \boldsymbol{\varepsilon}_{\boldsymbol{I}}^{(i)} \right) \mathrm{d}\Omega^{(i)} \right) & + \sum_{i=1}^{8} \left(\iint_{\Omega^{(i)}} \left(\frac{1}{2} \boldsymbol{\varepsilon}_{\boldsymbol{nl}}^{(i)^T} \boldsymbol{A}^{(i)} \boldsymbol{\varepsilon}_{\boldsymbol{nl}}^{(i)} \right) \mathrm{d}\Omega^{(i)} \right) \end{aligned} \tag{22}$$

As it could be observed in the above equation, the first term in the right-hand side of the above equation is linear function of the unknowns while the rest of the terms is quadratic, cubic and quartic functions of the unknowns, respectively. The linear term refers to the potential energy of applied loads. The quadratic energy comprises comes from the linear strain, curvature strain, shear strain vectors and also the initial imperfection effects. The cubic energy represents the coupling between linear and nonlinear strain vectors, the coupling between curvature and nonlinear strain vectors and also from initial imperfection effects. The quartic energy is only the effect of nonlinear strain vectors.

In the current study, all integrations have been taken numerically in which case each plate element is discretized by Chebyshev nodes. The total potential energy integration can be approximated by using equation below

$$\Pi^{(i)} = \iint_{\Omega^{(i)}} f(x, y) dx dy \approx \sum_{\zeta=1}^{n} \sum_{\eta=1}^{m} \varpi_\eta \omega_\zeta f(x_\eta, y_\zeta) \tag{23}$$

In which case η and ζ refer to the η^{th} node in *x*-direction and ζ^{th} node in *y*-direction and the coefficients ϖ_η and ω_ζ denote quadrature weights in *x* and *y*-directions, respectively. The Eq. (22) can be rephrased in a matrix form by using the Hessian technique.

$$\Pi = -\boldsymbol{d}^T \boldsymbol{V}_F + \frac{1}{2} \boldsymbol{d}^T (\boldsymbol{K}_{0P} + \boldsymbol{K}_0 + \boldsymbol{K}_{0s} + \boldsymbol{K}_{0I}) \boldsymbol{d} + \frac{1}{6} \boldsymbol{d}^T (\boldsymbol{K}_1 + \boldsymbol{K}_{1I}) \boldsymbol{d} + \frac{1}{12} \boldsymbol{d}^T \boldsymbol{K}_2 \boldsymbol{d} \tag{24}$$

where $\boldsymbol{V}_F$ is a column matrix of constants, including the effects of the applied loads. The column matrix $\boldsymbol{d}$ contains the unknowns of the problem. Subscripts P and I refer to the effects of penalty

terms and initial imperfection, respectively. Stiffness matrix of the plate is separated into $\boldsymbol{K}_0$, $\boldsymbol{K}_1$ and $\boldsymbol{K}_2$ matrixes which corresponding coefficients are constants, linear and quadratic functions of unknowns, respectively. Thus, the quantities on the right-hand side of the Eq. (24) represent linear, quadratic and cubic energy terms. Solution of the nonlinear problem is obtained by applying of the principle of minimum potential energy. Therefore, the unknown coefficients of the problem can be found by solving the following nonlinear equilibrium equations

$$\boldsymbol{F}(\boldsymbol{d}) = -\boldsymbol{V}_F + \left((\boldsymbol{K}_{0P} + \boldsymbol{K}_0 + \boldsymbol{K}_{0s} + \boldsymbol{K}_{0I}) + \frac{1}{2}(\boldsymbol{K}_1 + \boldsymbol{K}_{1I}) + \frac{1}{3}\boldsymbol{K}_2 \right) \boldsymbol{d} = \boldsymbol{0} \tag{25}$$

To obtain the solution of the above nonlinear algebraic equations, the quadratic extrapolation technique is used. In this study, in order to obtain the accurate results, the relevant convergence criterion has been defined based on the vector containing the unknown coefficients $(\boldsymbol{d})$. The iterative procedure is repeated until the following condition be satisfied.

$$\sqrt{\frac{\sum \Delta \boldsymbol{d}_i^2}{\sum \Delta \boldsymbol{d}_{i+1}^2}} < 5 \times 10^{-4} \tag{26}$$

where i is the iteration counter in extrapolation technique. Once the nonlinear equilibrium equations are solved and the unknown coefficients are found, it is possible to calculate the displacements, strains and stresses at any point in the perforated plate.

3. Numerical results and discussion

In this section, nonlinear behaviors for some composite laminates of dimensions $l \times l$, containing cutout with dimensions $a \times b$, are presented and investigated. Material properties of fiber and matrix have been given in Table 1. The chosen layup of laminate is $[0/45/-45/90]_2$ in this study and the value of l/h is chosen to be 20.

Table 1 Material properties of fiber and matrix (in MPa)

Component	E_1	E_2	v_{12}	G_{12}	G_{13}	G_{23}
Value	83000	5300	0.25	2500	2500	2500

Some results for moderately thick perforated plates have been validated by ABAQUS software in which, the plate is meshed, in average, with 3600 S4R shell elements. As mentioned before the boundary conditions are chosen to be simply supported on all edges and plates are subjected to in-plane compressive load $N_x$normal to the vertical edges $x = \pm l/2$. The results calculated in this paper are presented in dimensionless parametric terms of deflections and loads as follows:

Out-of-plane displacement: $W = w/h$

Longitudinal displacement at edge 2: $U = u/h$

Load parameter: $P = N_x\, l^2/E_2\, h^3$

Where, u and w are displacement components along *x* and *z* directions, respectively. To obtain the sufficient number of terms in the displacement fields of each plate-element, the convergence

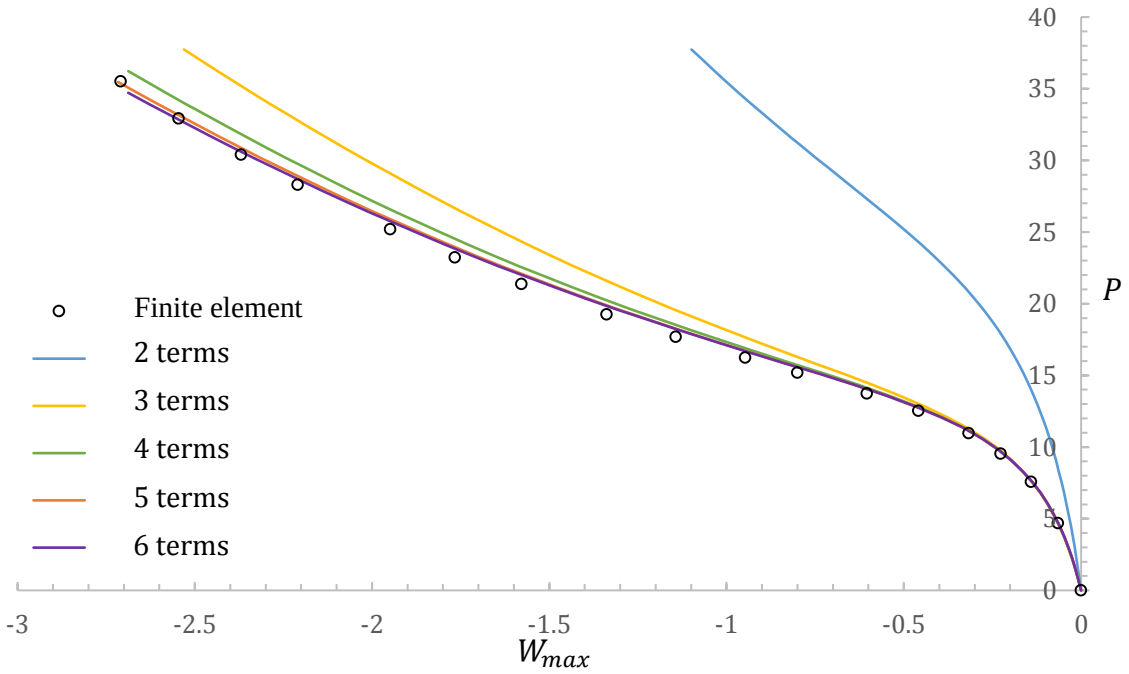

Fig. 4 Convergence study for composite plates containing square cutout $a = 0.5\ l$

study should be carried out for a perforated plate. In this case, a convergence study is conducted to analyze the nonlinear behavior of laminates containing square cutout with $a = b = 0.5\ l$. As it can be seen in Fig. 4, for this plate assembly, the convergence study with regard to the number of terms has discovered that 5×5 terms in each displacement field and for each plate-element are sufficient to obtain converged results which verified by finite element method.

The effect of cutout size for laminates with aforementioned boundary conditions is presented in Figs. 5-8. In Fig. 5 the out-of-plane deflection of perfect laminate with different square shaped cutout $a/l = 0.2, 0.3, 0.4, 0.5$ is presented. As it is seen, as the cutout enlarged the plate deflects more around the cutout edges. Also, as it can be seen in Fig. 6 for the aforementioned square cutout's sizes, the longitudinal displacement of the right edge of the laminate is shown and it can be observed that for plate containing larger cutout the nonlinear response is lower than those correspond to the smaller sizes.

However, in the case of rectangular cutouts, the position of the cutouts relative to the direction of loading, perpendicular to or along with, is a key factor in nonlinear response of perforated plates. In Figs. 7 and 8, the nonlinear responses of composite laminates containing rectangular cutouts are presented, the term X displayed in these two figures is equal to a/l or b/l which is chosen to be $0.1, 0.2, 0.3$ and 0.4. The load-deflection behavior has been shown in Fig. 7 while the behavior of load versus longitudinal displacement is presented in Fig. 8. As it can be observed in Fig. 7, in the case of vertical cutout (i.e. the cutout is aligned perpendicular to the loading direction) for $b/l = 0.1$ and 0.2, the out-of-plane deflection of the bottom of the cutout is lower than a perfect plate although, by the cutout getting larger the bottom of the cutout deflects more. However, in the case of horizontal cutout, i.e. cutout aligned along the loading direction, the nonlinear response is

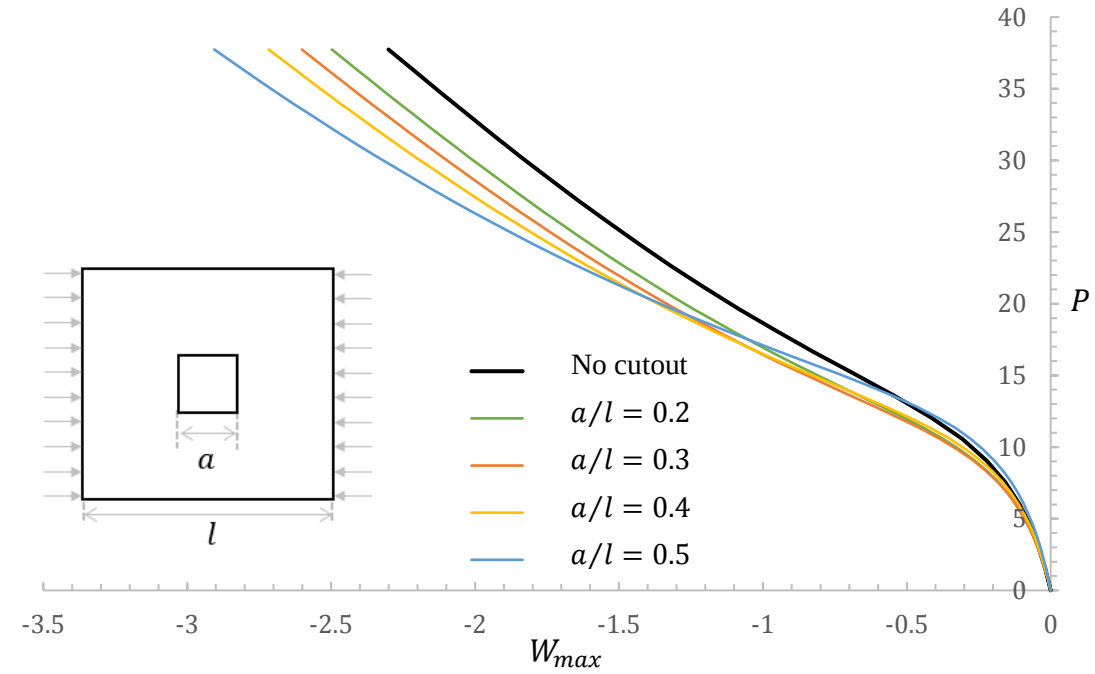

Fig. 5 Effect of cutout size on load-deflection response of composite laminates containing square cutout

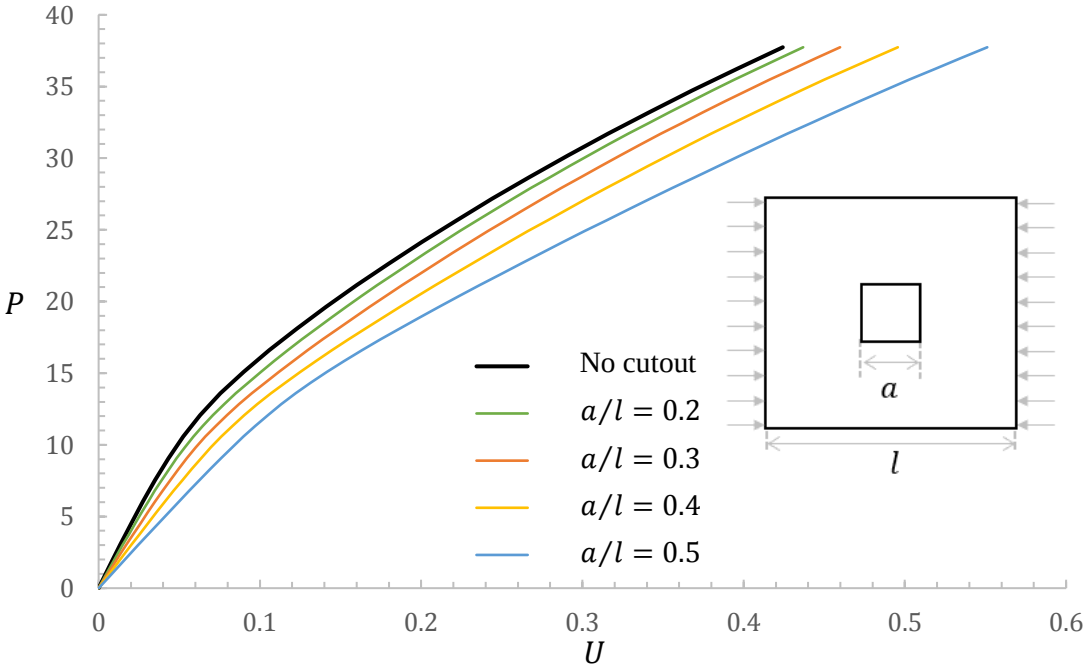

Fig. 6 Effect of cutout size on load-longitudinal displacement behavior of composite laminates containing square cutout

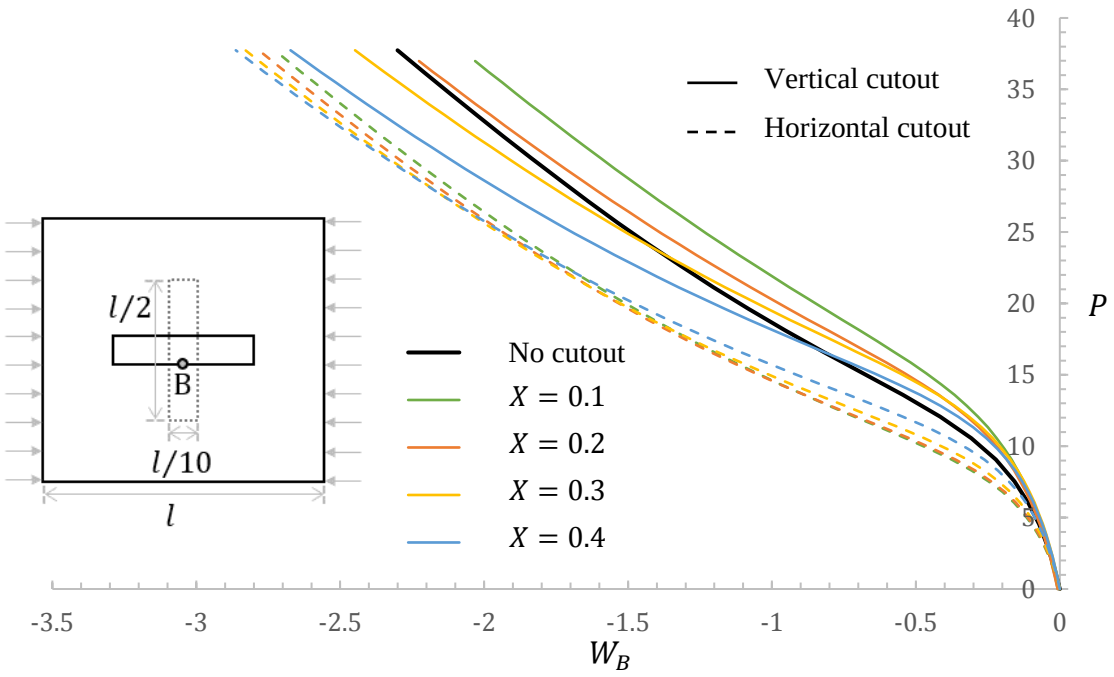

Fig. 7 Effect of cutout size on out-of-plane deflection of cutout in composite laminate containing rectangular cutouts

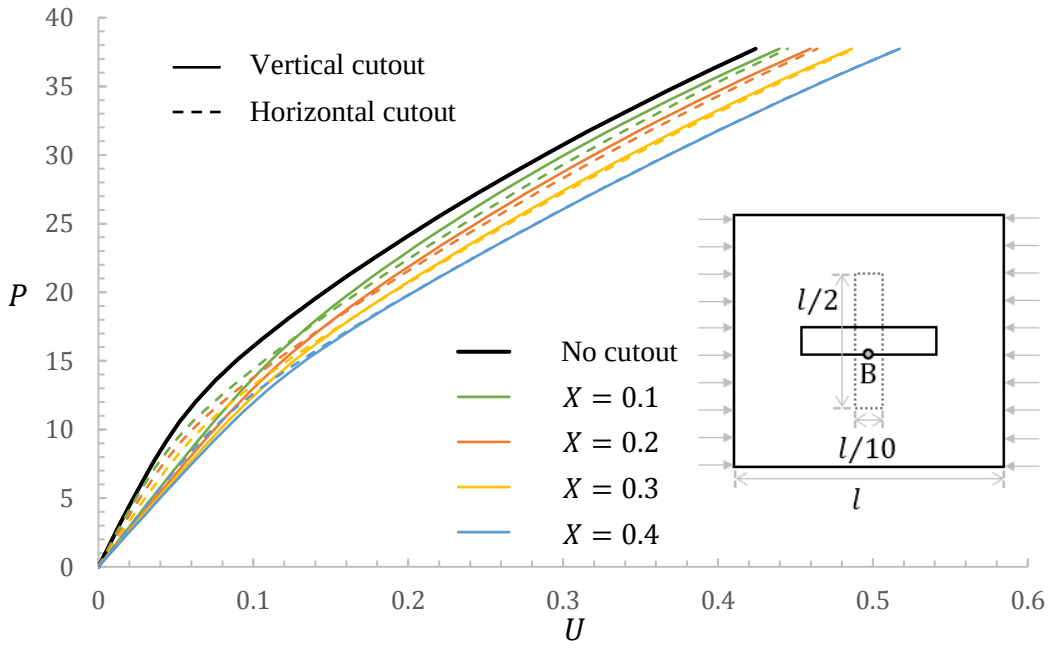

Fig. 8 Effect of cutout size on load-longitudinal displacement behavior of laminates containing rectangular cutouts

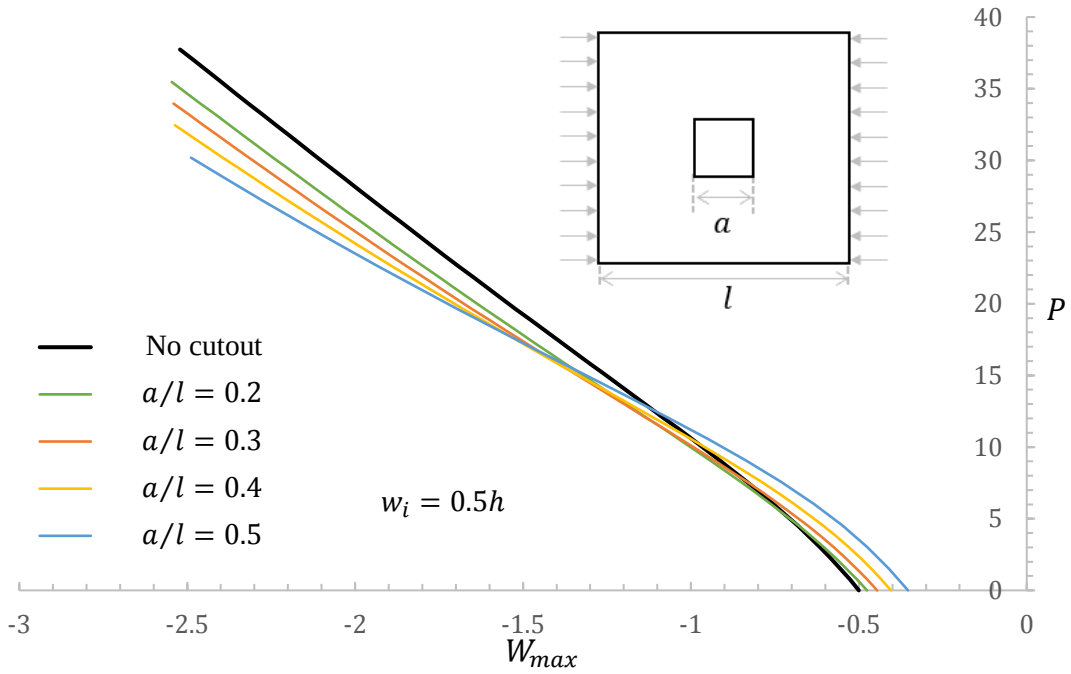

Fig. 9 Effect of cutout size on nonlinear behavior of laminates with initial geometric imperfection containing square cutout

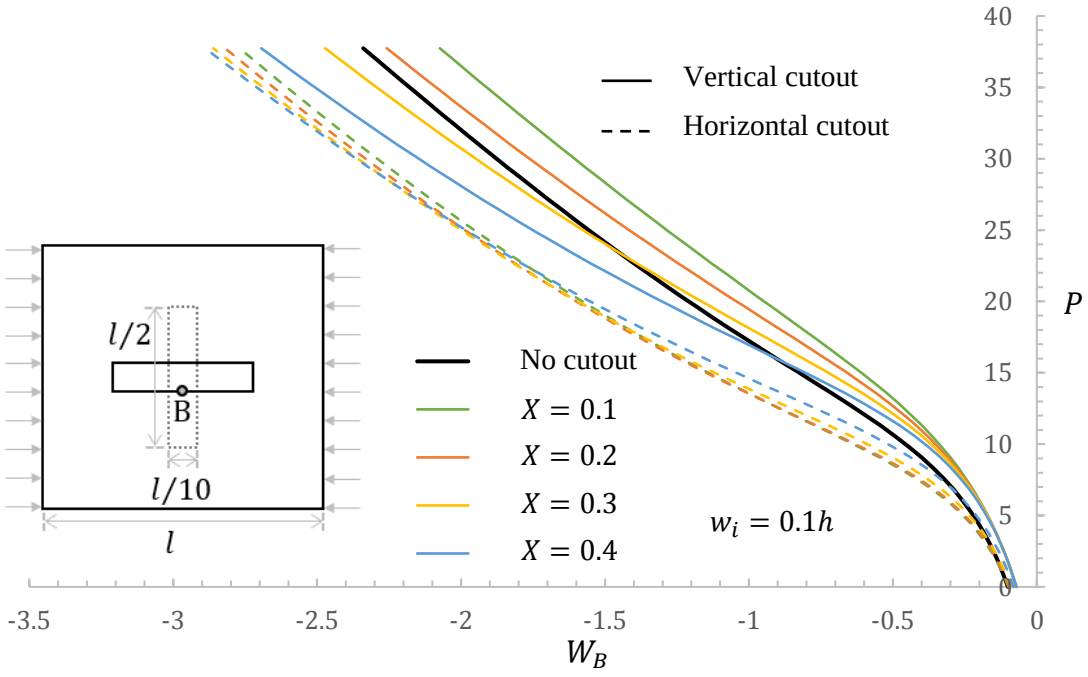

Fig. 10 Effect of cutout size on nonlinear behavior of imperfect laminates containing rectangular cutout

obtained lower than the perfect plate. It means that at the same level of loading, plates having horizontal cutouts, have larger deflections. Nevertheless, the effects of cutout orientation with respect to loading direction is undeniable. It can be also concluded from Fig. 8 that the stiffness of the plates containing cutout (horizontally or vertically) is generally lower than the perfect laminates but for the same aspect ratios of the holes, this reduction in stiffness is almost similar.

As it mentioned before, in this study the nonlinear behavior of perforated laminates with initial geometric imperfection are also investigated and discussed. To model the cutout in this study, a sinusoidal cutout shape has been assumed in which the maximum value w_i is placed at the center of the laminate. The results of laminates containing square cutout with different sizes are presented in Fig. 9 when they have an initial imperfection of $w_i = 0.5h$. As it is seen, the plates containing larger cutout, deflect more than perfect plate and plate with smaller cutout. Nonlinear responses of laminates with smaller initial imperfection $w_i = 0.1h$ and with both rectangular and horizontal cutouts, have been displayed in Fig. 10. There is a similar conclusion to Fig. 7 for this figure.

7. Conclusions

In the current study, a new methodology was used to investigate the nonlinear behavior of composite plates with or without initial geometric imperfection containing square/rectangular cutout under in-plane compressive load. The governing equations were based on the first-order shear deformation theory and Von-Karman assumptions. Approximation of the displacement fields were based on the Ritz method and by Chebyshev polynomials. The penalty method was used to assemble the plate-element and therefore the whole plate potential energy was the summation of potential energy of the elements. The principle of minimum potential energy was used to obtain the imperfect laminate equilibrium equations and the quadratic extrapolation technique was carried out to calculate the unknowns and displacements. Some results with regards to the cutout size and shape were obtained and presented in non-dimensional graphical forms. The results indicated the ability of the proposed method in obtaining nonlinear results for composite plates containing square/rectangular holes for which the laminates had an initial geometrical imperfection. An important conclusion was that the direction of the loading relative to the position of rectangular cutout may affect deeply the nonlinear behavior of imperfect laminates.

References

Baba, B.O. and Baltaci, A. (2007), "Buckling characteristics of symmetrically and antisymmetrically laminated composite plates with central cutout", *Appl. Compos. Mater.*, **14**, 265-276.

Bakhshi, N. and Taheri-Behrooz, F. (2019), "Length effect on the stress concentration factor of a perforated orthotropic composite plate under in-plane loading", *Compos. Mater. Eng.*, **1**(1), 71-90.

Britt, V.O. (1994), "Shear and compression buckling analysis for anisotropic panels with elliptical cutouts", *AIAA J.*, **32**(11), 2293-2299.

Brubak, L. and Hellesland, J. (2007), "Semi-analytical postbuckling and strength analysis of arbitrarily stiffened plates in local and global bending", *Thin Wall. Struct.*, **45**(6), 620-633.

Cetkovic, M. and Vuksanovic, Dj. (2011), "Large deflection analysis of laminated composite plates using layerwise displacement model", *Struct. Eng. Mech.*, **40**(2), 257-277.

Chia, C.Y. (1988), "Geometrically nonlinear behavior of composite plates: a review", *Appl. Mech. Rev.*, **41**(12), 439-451.

Eiblmeier, J. and Loughlan, J. (1995), "The buckling response of carbon fiber composite panels with reinforced cut-outs", *Compos. Struct.*, **32**, 97-113.
Ghannadpour, S.A.M. and Karimi, M. (2018), "Domain decomposition technique to simulate crack in nonlinear analysis of initially imperfect laminates", *Struct. Eng. Mech.*, **68**(5), 603-619.
Ghannadpour, S.A.M. and Kiani, P. (2018), "Nonlinear spectral collocation analysis of imperfect functionally graded plates under end-shortening", *Struct. Eng. Mech.*, **66**(5), 557-568.
Ghannadpour, S.A.M. and Mehrparvar, M. (2018), "Energy effect removal technique to model circular/elliptical holes in relatively thick composite plates under in-plane compressive load", *Compos. Struct.*, **202**, 1032-1041.
Ghannadpour, S.A.M. and Ovesy, H.R. (2009), "The application of an exact finite strip to the buckling of symmetrically laminated composite rectangular plates and prismatic plate structures", *Compos. Struct.*, **89**(1), 151-158.
Ghannadpour, S.A.M., Karimi, M. and Tornabene, F. (2019), "Application of plate decomposition technique in nonlinear and post-buckling analysis of functionally graded plates containing crack", *Compos. Struct.*, **220**, 158-167.
Ghannadpour, S.A.M., Najafi, A. and Mohammadi, B. (2006), "On the buckling behavior of cross-ply laminated composite plates due to circular/elliptical cutouts", *Compos. Struct.*, **75**, 3-6.
Ghannadpour, S.A.M., Ovesy, H.R. and Zia-Dehkordi, E. (2015), "Buckling and post-buckling behaviour of moderately thick plates using an exact finite strip", *Compos. Struct.*, **147**, 172-180.
Ghannadpour, S.A.M., Shakeri, M. and Barvaj, A.K. (2018), "Ultimate strength estimation of composite plates under combined in-plane and lateral pressure loads using two different numerical methods", *Steel Compos. Struct.*, **29**(6), 785-802.
Jain, P. and Kumar, A. (2004), "Postbuckling response of square laminates with a central circular/elliptical cutout", *Compos. Struct.*, **65**, 179-185.
Kandasamy, R., Dimitri, R. and Tornabene, F. (2016), "Numerical study on the free vibration and thermal buckling behavior of moderately thick functionally graded structures in thermal environments", *Compos. Struct.*, **157**, 207-221.
Kar, V.R., Panda, S.K. and Mahapatra, T.R. (2016), "Thermal buckling behaviour of shear deformable functionally graded single/doubly curved shell panel with TD and TID properties", *Adv. Mater. Res.*, **5**(4), 205-221.
Katariya, P.V. and Panda, S.K. (2016), "Thermal buckling and vibration analysis of laminated composite curved shell panel", *Aircraft Eng. Aerosp. Technol.*, **88**(1), 97-107.
Katariya, P.V., Panda, S.K., Hirwani, C.K., Mehar, K. and Thakare, O. (2017), "Enhancement of thermal buckling strength of laminated sandwich composite panel structure embedded with shape memory alloy fiber", *Smart Struct. Syst.*, **20**(5), 595-605.
Komur, M.A. and Sonmez, M. (2008), "Elastic buckling of rectangular plates under linearly varying in-plane normal load with a circular cutout", *Mech. Res. Commun.*, **35**, 361-371.
Komur, M.A., Sen, F., Ataş, A. and Arslan, N. (2010), "Buckling analysis of laminated composite plates with an elliptical/circular cutout using FEM", *Adv. Eng. Softw.*, **41**, 161-164.
Kong, C.W., Hong, C.S. and Kim, C.G. (2001), "Postbuckling strength of composite plate with a hole", *J. Reinf. Plast. Compos.*, **20**(6), 466-481.
Leissa, A.W. (1987), "A review of laminated composite plate buckling", *Appl. Mech. Rev.*, **40**, 575-591.
Liew, K.M., Wang, J., Ng, T.Y. and Tan, M.J. (2004), "Free vibration and buckling analysis of shear-deformable plates based on FSDT meshfree method", *J. Sound Vib.*, **276**, 997-1017.
Madenci, E. and Barut, A. (1994), "Pre- and postbuckling response of curved, thin, composite panels with cutouts under compression", *Int. J. Numer. Meth. Eng.*, **37**, 1499-1510.
Mehrparvar, M. and Ghannadpour, S.A.M. (2018), "Plate assembly technique for nonlinear analysis of relatively thick functionally graded plates containing rectangular holes subjected to in-plane compressive load", *Compos. Struct.*, **202**, 867-880.
Mohammadi, B., Najafi, A. and Ghannadpour, S.A.M. (2006), "Effective widths of compression-loaded of perforated cross-ply laminated composites", *Compos. Struct.*, **75**, 7-13.

Nemeth, M.P. (1990), "Buckling and postbuckling behavior of square compression-loaded graphite-epoxy plates with circular cutouts", Technical Paper 3007, NASA.

Noor, A.K. and Peters, J.M. (1994), "Finite element buckling and postbuckling solutions for multilayered composite panels", *Finite Elem. Anal. Des.*, **15**, 343-367.

Ovesy, H.R. and Ghannadpour, S.A.M. (2011), "An exact finite strip for the initial postbuckling analysis of channel section struts", *Compos. Struct.*, **89**(19), 1785-1796.

Ovesy, H.R., Zia-Dehkordi, E. and Ghannadpour, S.A.M. (2016), "High accuracy post-buckling analysis of moderately thick composite plates using an exact finite strip", *Compos. Struct.*, **174**, 104-112.

Panda, S.K. and Singh, B.N. (2009), "Thermal post-buckling behaviour of laminated composite cylindrical/hyperboloid shallow shell panel using nonlinear finite element method", *Compos. Struct.*, **91**(3), 366-374.

Panda, S.K. and Singh, B.N. (2010), "Thermal post-buckling analysis of a laminated composite spherical shell panel embedded with shape memory alloy fibers using non-linear finite element method", *Proc. Inst. Mech. Eng., Part C: J. Mech. Eng. Sci.*, **224**(4), 757-769.

Panda, S.K. and Singh, B.N. (2013), "Post-buckling analysis of laminated composite doubly curved panel embedded with SMA fibers subjected to thermal environment", *Mech. Adv. Mater. Struct.*, **20**(10), 842-853.

Reddy, J.N. (2004), *Mechanics of Laminated Composite Plates and Shells: Theory and Analysis*, CRC Press, Boca Raton, U.S.A.

Şahin, Ö.S. (2005), "Thermal buckling of hybrid angle-ply laminated composite plates with a hole", *Compos. Sci. Technol.*, **65**, 1780-1790.

Tounsi, A., Atmane, H.A., Khiloun, M., Sekkal, M., Taleb, O. and Bousahla, A.A. (2019), "On buckling behavior of thick advanced composite sandwich plates", *Compos. Mater. Eng.*, **1**(1), 1-19.

Vandenbrink, D.J. and Kamat, M.P. (1987), "Post-buckling response of isotropic and laminated composite square plates with circular holes", *Finite Elem. Anal. Des.*, **3**, 165-174.

Yang, Q.J. and Hayman, B. (2015), "Prediction of post-buckling and ultimate compressive strength of composite plates by semi-analytical methods", *Eng. Struct.*, **84**, 42-53.

Yang, Q.J., Hayman, B. and Osnes, H. (2013), "Simplified buckling and ultimate strength analysis of composite plates in compression", *Compos. Part B: Eng.*, **54**, 343-352.

CC